Global-scale Multidecadal Variability Missing in State-of-the-Art Climate Models

UNIVERSITY of WISCONSIN UWMILWAUKEE College of Letters and Science ATMOSPHERIC SCIENCE DEPARTMENT OF MATHEMATICAL SCIENCES

Sergey Kravtsov[1,2], Christian Grimm[1], Shijie Gu[1]

[1]Department of Mathematical Sciences, Atmospheric Science Group, University of Wisconsin-Milwaukee, P.O. Box 413, Milwaukee, WI 53201

[2]Additional affiliation: P. P. Shirshov Institute of Oceanology, Russian Academy of Sciences

AGU 100 FALL MEETING Washington, D.C. | 10-14 Dec 2018

Session: GC33H:The Rate of Global Warming on Decadal to Multidecadal time scales; Presentation: GC33H-1446; Display time: Wed., December 12th, 13:40 - 18:00

Main ideas

We apply optimal (Wiener) filtering to identify non-stationary (secular) climate variability in the observed and simulated (spatially extended, gridded) surface temperatures (SATs) and to study the differences between the two. Each non-stationary SAT signal is defined to be associated with the part of the SAT singular spectrum (inferred via Multi-channel Singular Spectrum Analysis —M-SSA: Ghil et al. 2002) that cannot be simulated by stationary linear inverse models (Penland 1989, 1996; Kravtsov et al. 2005) trained on pre-low-pass filtered data. The filter weights are then derived via computing the signal-to-noise ratio of each M-SSA mode, and the weighted M-SSA decomposition is transformed back to physical space to reconstruct the part of variability associated with the signal (**Fig. 1**).

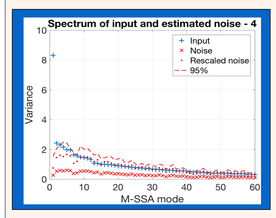

Fig. 1: M-SSA spectra associated with run 4 from the LENS project. The raw spectrum of input signal (blue plus signs) matches the rescaled noise spectrum (red dots) very well in the tail of the spectrum. Only two leading input modes, however, exceed the 95th percentile of the variance associated with the stationary noise model and will be used to reconstruct the secular signal in this simulation.

Examples using LENS simulations

We first verified our methodology using the simulations from the Community Earth System Model (CESM) Large Ensemble Project (LENS) [Kay et al., 2015]. Forty available simulations of the twentieth century variability reflect a common forced signal summed with independent realizations of internal climate variability. Each SAT simulation was filtered as described above. We then compared the non-stationary signals so estimated with forced signal defined via the ensemble average of the surface temperature over all of the 40 simulations. The reconstructed non-stationary signal closely resembles the low-frequency forced response of the CESM model, but fails to capture the temperature response to episodic volcanic eruptions (**Fig. 2**). The secular *internal* variability in LENS simulations is, therefore, relatively small.

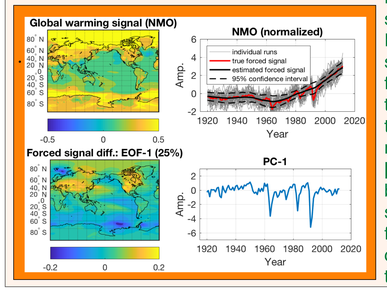

Fig. 2: Analysis of LENS simulations: **[Top]** Estimated non-stationary signal reflects low-frequency component of the forced variability in the Northern Hemisphere mean temperature (NMO). **[Bottom]** The difference between estimated non-stationary signal and true forced signal is dominated by response to volcanic eruptions.

Observed and CMIP5 simulated variability

In the main part of our analysis, we considered 17 ensembles of the CMIP5 model simulations [Taylor et al., 2012] (with the total of 111 simulations), as well as gridded surface temperature product from NOAA's twentieth century reanalysis (20CR) [Compo et al., 2011] in lieu of the observed SATs. Similarly to LENS simulations, the non-stationary signals inferred from CMIP5 models capture the low-frequency forced signal less the effect of volcanic aerosols; however, when considered in aggregate, they reflect a larger spread of possible secular signals due to incorporation of model uncertainty (not shown). On the other hand, the dynamical structure of the secular signal in observations is richer than that in the models in the sense of being represented by a larger number of significant M-SSA modes (not shown).

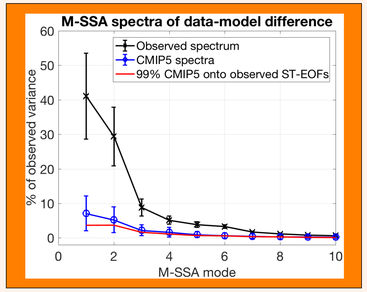

Fig. 3: M-SSA spectra of data–models secular difference (black); the error bars show standard uncertainty computed over 111 estimates. Also shown are M-SSA spectra of model signals' deviations from individual model ensemble means (blue), and the 99th percentile of variances obtained by projecting the simulated signals onto the observed ST-EOFs of M-SSA analysis (red).

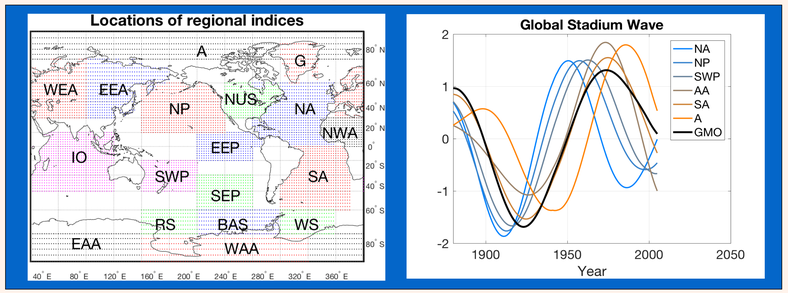

Fig. 4: Observed global stadium wave: **[Left]** locations of regional SAT indices. **[Right]** Reconstructed time series associated with the leading M-SSA pair in select regional indices. GMO (Global Multidecadal Oscillation) time series represents the reconstruction of the global-mean temperature. All time series are dimensionless; the actual standard deviations of A and AA indices is around 0.6K; that of all others – 0.1K.

Global Multidecadal Oscillation

Given that our estimated secular signals in CMIP5 simulations primarily reflect the forced response of CMIP5 models, it makes sense to linearly subtract them from the observed secular signal to study the part of the observed secular variability unaccounted for in CMIP5 simulations (Steinman et al. 2015; Kravtsov and Callicutt 2017; Kravtsov 2017). We can also subtract the individual model ensemble-mean secular signals from all of this model's simulations to define internal component of the secular signal in each simulation. **The M-SSA analysis of data–model differences identifies a pronounced pair of M-SSA modes altogether absent from model simulations (Fig. 3)**. The reconstruction of this pair of modes for regional climate indices (**Fig. 4**) identifies a multidecadal oscillation propagating across the climate index network — a so-called *stadium wave* (Wyatt et al. 2012), which we will refer to as the **Global Stadium Wave** or **Global Multidecadal Oscillation**. The phasing of the indices in the global stadium wave is consistent with Kravtsov (2017) [not shown].

The order of indices in the sequence of Fig. 4 (except for GMO) is chosen based on the visual analysis of the SAT anomaly propagation over a time period between 1921 and 1963, which roughly spans half of the oscillation period **(Fig. 5)**. In year 1921, the oscillation is in its cold phase (cf. Fig. 4), with the exception of four major positive SAT anomaly spots: west of Weddell Sea, in eastern equatorial Pacific, as well as over central US and Greenland. The development of an oscillation starts with emergence of the positive SST anomaly in the North Atlantic (1921–30), which subsequently expands and growth along with SST anomalies in North and Southwestern Pacific (1933–1942), then Southern Ocean and Antarctica (1941–1957) and, finally, over Arctic (1960–1963), at which point the oscillation arrives at its positive phase throughout the world (less four major negative SAT anomaly regions roughly at the same locations as their positive analogs 40 years ago).

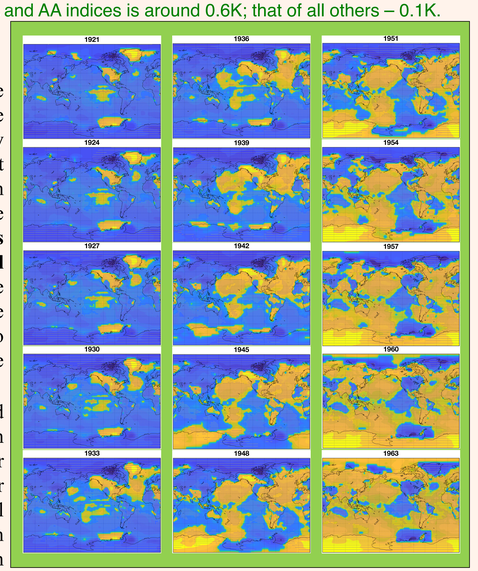

Fig. 5: A 1921–1963 segment of the global stadium wave; shown are reconstructed SAT anomalies raised to the power of 1/7, which alleviates differences between SAT anomalies over ocean and over land to concentrate on the anomaly patterns and their propagation. Color axis is from –1.5 (saturated blue) to 1.5 (saturated yellow).

Discussion

The key result of this study is the identification of a pronounced global-scale mode of multidecadal climate variability in the twentieth century which is not captured by any of the state-of-the-art climate models considered. Such a mode was previously proposed to explain a major fraction of variability in a network of oceanic and atmospheric climate indices over the Northern Hemisphere and termed the stadium wave (Wyatt et al. 2012; Kravtsov et al. 2014, Kravtsov 2017). Here we show that this mode has a global significance and provide a description of its worldwide evolution throughout the twentieth century.

The global stadium wave presented here was defined in terms of deviations of the observed surface temperature from the secular trends identified in CMIP5 models, which can be interpreted to be proxies for the observed forced signal. In principle, it is still possible that these deviations are pronounced in part because of the potential biases in the CMIP5 derived forced signals. However, the oscillatory character of the global stadium wave and the spatial pattern of its delayed teleconnections strongly suggest that this mode reflects internal climate variability, perhaps associated with that of global oceanic conveyor-belt circulation. In either case, climate modeling efforts should strive to alleviate discrepancies between the observed and simulated multidecadal climate variability.

References

Ghil, M., et al., 2002. *Reviews of Geophysics*, **40**, 1003.

Kravtsov, S., et al., 2005. *J. Climate*, **18**, 4404–4424.

Kravtsov, S., et al. 2014. *Geophys. Res. Lett.*, **41**, 6881–6888.

Kravtsov, S., 2017. *Geophys. Res. Lett.*, **44**, 5749–5757.

Kravtsov. S., and D. Callicutt, 2017. *Inter. J. Climat.*, **37**, 4417–4433.

Penland. C., 1989. *Mon. Wea. Rev.*, **117**, 2165–2185.

Penland, C., 1996. *Physica D*, **98**, 534–558.

Steinman, B. A., et al., 2015. *Science*, **347**, 988–991.

Taylor, K. E., et al., 2012. *Bull. Am. Meteorol. Soc.*, **93**, 485–498.

Wyatt, M. G., et al., 2012. *Clim. Dyn.*, **38**, 929–949.

Acknowledgments

We acknowledge the World Climate Research Programme's Working Group on Coupled Modeling, which is responsible for CMIP, and we thank the climate modeling groups for producing and making available their model output. This research was supported by the NSF grant AGS-1408897, Russian Ministry of Education and Science (project #14.W03.31.0006), as well as by contract #18-12-00231 of the Russian Science Fondation.

For further information

Please contact *kravtsov@uwm.edu*. A PDF version of this poster and complementary animations can be found at Sergey Kravtsov's UWM website — https://people.uwm.edu/kravtsov/presentations/